

This is the accepted manuscript made available via CHORUS. The article has been published as:

Bulk Fermi surface and momentum density in heavily doped $\text{La}_{2-x}\text{Sr}_x\text{CuO}_4$ using high-resolution Compton scattering and positron annihilation spectroscopies

W. Al-Sawai, B. Barbiellini, Y. Sakurai, M. Itou, P. E. Mijnders, R. S. Markiewicz, S. Kaprzyk, S. Wakimoto, M. Fujita, S. Basak, H. Lin, Yung Jui Wang, S. W. H. Eijt, H. Schut, K. Yamada, and A. Bansil

Phys. Rev. B **85**, 115109 — Published 13 March 2012

DOI: [10.1103/PhysRevB.85.115109](https://doi.org/10.1103/PhysRevB.85.115109)

Bulk Fermi surface and momentum density in heavily doped $\text{La}_{2-x}\text{Sr}_x\text{CuO}_4$ using high resolution Compton scattering and positron annihilation spectroscopies

W. Al-Sawai¹, B. Barbiellini¹, Y. Sakurai², M. Itou², P. E. Mijnders^{1,3}, R. S. Markiewicz¹, S. Kaprzyk^{1,4}, S. Wakimoto⁵, M. Fujita⁶, S. Basak¹, H. Lin¹, Yung Jui Wang¹, S.W.H. Eijt³, H. Schut³, K. Yamada^{6,7}, and A. Bansil¹

¹*Department of Physics, Northeastern University, Boston, MA 02115, USA.*

²*Japan Synchrotron Radiation Research Institute (JASRI),
SPring-8, 1-1-1 Kouto, Sayo, Hyogo 679-5198, Japan.*

³*Department of Radiation, Radionuclides & Reactors, Faculty of Applied Sciences,
Delft University of Technology, Delft, The Netherlands.*

⁴*Academy of Mining and Metallurgy AGH, 30059 Krakow, Poland.*

⁵*Quantum Beam Science Directorate, Japan Atomic Energy Agency, Tokai, Naka, Ibaraki 319-1195, Japan.*

⁶*Institute of Materials Research, Tohoku University, Sendai 980-8577, Japan.*

⁷*Advanced Institute of Materials Research, Tohoku University, Sendai 980-8577, Japan.*

(Dated: February 14, 2012)

We have observed the bulk Fermi surface (FS) in an overdoped ($x=0.3$) single crystal of $\text{La}_{2-x}\text{Sr}_x\text{CuO}_4$ by using Compton scattering. A 2-D momentum density reconstruction from measured Compton profiles yields a clear FS signature in the third Brillouin zone along [100]. The quantitative agreement between density functional theory (DFT) calculations and momentum density experiment suggests that Fermi-liquid physics is restored in the overdoped regime. In particular the predicted FS topology is found to be in good accord with the corresponding experimental data. We find similar quantitative agreement between the measured 2D angular correlation of positron annihilation radiation (2D-ACAR) spectra and the DFT based computations. However, 2D-ACAR does not give such a clear signature of the FS in the extended momentum space in either the theory or the experiment.

PACS numbers: 74.72-h, 78.70.Ck, 78.70.Bj, 71.10.Ay

I. INTRODUCTION

High temperature cuprate superconductors^{1,2} such as $\text{La}_{2-x}\text{Sr}_x\text{CuO}_4$ (LSCO) show interesting Mott insulator behavior^{3,4} at low doping x while at high doping these materials display Fermi liquid properties.^{1,5,6} This fascinating phase diagram is complicated by the presence of various inhomogeneities such as stripe ordering⁷ and possible clustering of dopants.⁸ Many models of the overdoped metallic phase have been put forward, some generalizing the concept of the Fermi liquid, while others attempt to use Hubbard or t-J models. In this context, it is important to investigate the electron momentum density of these materials, which, when compared to predictions of theoretical models, can give an indication of their correctness or applicability.

Insight into the evolution of electronic states can be obtained via Fermi surface (FS) measurements in various doping regimes. Experimental FS work on the cuprates has to date been limited mainly to angle-resolved photoemission (ARPES),^{1,2} quantum oscillations (QO),⁹ and scanning tunneling spectroscopies (STS).¹⁰ However, ARPES¹¹ and STS¹² are surface sensitive probes. Although QO measurements probe the bulk, they provide only FS areas without giving information on the location of the FSs in momentum space. Furthermore QO require long mean free paths and large magnetic fields which could alter the ground state. For underdoped sam-

ples there is evidence of FSs distorted from Local Density Approximation (LDA) based band structure predictions, involving arcs or pockets, but as doping is increased it appears that a large, LDA-like FS becomes manifest as the pseudogap collapses near optimal doping. For an overdoped Tl-cuprate, the FS has been found to be large and closed around (π, π) ,¹³ suggesting that the Van Hove singularity (vHS) still lies below the Fermi energy E_F in good agreement with LDA calculations.¹⁴

These considerations provide motivation for deploying genuinely bulk sensitive spectroscopies for FS measurements in the cuprates. Two such spectroscopies, which have been used extensively for this purpose, are high-resolution Compton scattering^{15,16} and two-dimensional angular correlation of positron annihilation radiation (2D-ACAR).¹⁷⁻¹⁹ Compton scattering probes the momentum density of the many-body electronic ground state of the system and is *insensitive* to the presence of defects or surfaces in the sample.²⁰ 2D-ACAR also probes the bulk momentum density, but its interpretation can be complicated by positron spatial distribution effects.²¹⁻²³ On the other hand, the Compton scattering technique requires large single crystals of materials having atoms with high atomic numbers ($Z \sim 30$), as is the case for all cuprates, but it suffers from the problem of a relatively low signal from valence electrons sitting on the large background contribution from the core electrons.

With this background, the present article reports a

study of the FS and electron momentum density (EMD) of an overdoped single crystal of $\text{La}_{2-x}\text{Sr}_x\text{CuO}_4$ (LSCO) for the hole doping level $x=0.3$. Compton scattering and 2D-ACAR experiments have been carried out on the same LSCO sample, and the results are analyzed through parallel computations of the FS, the EMD as well as the electron-positron momentum density within the framework of DFT. The conventional picture of the metallic state based on Landau Fermi liquid theory is expected to become increasingly viable with doping as the system becomes more weakly correlated, even though the physics of the cuprates is generally dominated by deviations from such a simple picture of electronic states. For this reason, the overdoped LSCO provides a good starting system for investigating the fermiology of the cuprates.

To our knowledge, this is the first attempt to study the FS of LSCO using high-resolution Compton scattering experiments, although earlier Compton studies have provided some insight into the ground-state momentum density and electron correlation effects in LSCO.^{24,25} The 2D-ACAR experiments, on the other hand, have been deployed successfully by several groups in the past for delineating the FSs of the cuprates in a number of favorable cases.²¹

Here, by measuring a series of high resolution Compton profiles, we reconstruct the 2D momentum density in overdoped LSCO and identify a clear signature of the FS in the third Brillouin zone. Moreover, the DFT-based theoretical EMD is found to be in quantitative accord with the Compton scattering results, indicating that the ground state wavefunction in the overdoped system is well-described by the weakly correlated DFT picture. We have also found a quantitative level of agreement between the measured and computed 2D-ACAR spectra. However, the 2D-ACAR spectra do not reveal clear FS signatures due to the well-known positron spatial distribution effects, which can make the positron insensitive to electrons in the Cu-O planes.

The remainder of this article is organized as follows. Section II describes experimental details of sample preparation and of Compton scattering and positron-annihilation experiments. Section III provides technical details of our DFT-based EMD, FS and electron-positron momentum density computations. Section IV discusses momentum density anisotropy results, while Sec. V considers the FS determination. The article concludes with a summary of the results in Sec. VI.

II. EXPERIMENTS

The heavily overdoped single crystal ($x = 0.30$) was grown by the traveling solvent floating zone method. For this purpose, a powder sample was first synthesized by the conventional solid state reaction method. It was then shaped into feed rods under hydrostatic pressure and sintered at 1173 K for 12 hours, and at 1423 K for an additional 10 hours. In this process, excess CuO of 2 mol%

was added to the feed rods to compensate for the evaporation of CuO during the high temperature process. The grown crystal was subsequently annealed under an oxygen pressure of 3 atm at 1173 K for 100 hours. SQUID measurements, using MPMS-XL5HG (Quantum Design, Inc.), showed no superconductivity down to 2 K. Neutron diffraction studies indicated that the crystal is tetragonal ($I4/mmm$) down to the lowest temperature. The crystal was also characterized by other experiments.²⁶⁻²⁸

We have measured 10 Compton profiles with scattering vectors equally spaced between the $[100]$ and $[110]$ directions using the Cauchois-type x-ray spectrometer at the BL08W beamline of SPring-8.²⁹ All measurements were carried out at room temperature. The overall momentum resolution is estimated to be 0.13 a.u. full-width-at-half-maximum (FWHM). The incident x-ray energy was 115 keV and the scattering angle was 2.88 rad. Approximately 5×10^5 counts in total were collected at the Compton peak channel, and two independent measurements were performed in order to check the results. Each Compton profile was corrected for absorption, analyzer and detector efficiencies, scattering cross section, possible double scattering contributions, and x-ray background. The core-electron contributions were subtracted from each Compton profile. A two-dimensional momentum density, representing a projection of the three-dimensional momentum density onto the (ab) -plane, was reconstructed from each set of ten Compton profiles using the direct Fourier transform method.³⁰

The 2D-ACAR was measured using the Delft University 2D-ACAR spectrometer³¹ with a conventional ^{22}Na positron source. The data were taken at a temperature of about $T=70\text{K}$. To correct for the sample shape ($5.7 \times 3.5 \times 4.5 \text{ mm}^3$) the data were convoluted with a gaussian of FWHM of 0.1 channel in the x direction and 1.7 channels in the y direction (along which the positrons impinge on the sample), where 1 channel corresponds to 0.184 mrad. The total resolution is $1.0 \times 1.0 \text{ mrad}^2$ FWHM (1 mrad = 0.137 a.u.). The total number of coincidences collected is 76.3×10^6 and the maximum number of coincidences at the center is 16.7×10^3 counts.

The effects of superconductivity on the 2D-ACAR as well as Compton spectra³² are expected to be below the resolution of the current experiments. For this reason, we have not carried out experiments on the superconducting state in connection with the present study.

III. CALCULATIONS

Our electronic structure calculations are based on the LDA within the framework of the DFT. An all-electron fully charge-self-consistent semi-relativistic Korringa-Kohn-Rostoker (KKR) methodology was used.³³ The crystal structure of LSCO was taken to be body-centered tetragonal (BCT) with space group $I4/mmm$ (139) us-

ing lattice parameters a and c given in Ref. 34. A non-spinpolarized calculation neglecting the magnetic structure was performed. Self-consistency was obtained for $x = 0$ and the effect of doping was treated within a rigid band model by shifting the Fermi energy to accommodate the proper number of electrons.^{35–37} The results are in good agreement with other calculations.³⁸ The formalism for computing momentum density, $\rho(\mathbf{p})$, is discussed in Refs. 39–42. The EMD is calculated according to the formula

$$\rho(\mathbf{p}) = \sum_i n_i(\mathbf{k}) \left| \int \exp(-i\mathbf{p}\cdot\mathbf{r}) \psi_i(\mathbf{r}) d\mathbf{r} \right|^2 \quad (1)$$

and the ACAR spectrum is computed as

$$\rho^{2\gamma}(\mathbf{p}) = \sum_i n_i(\mathbf{k}) \left| \int \exp(-i\mathbf{p}\cdot\mathbf{r}) \psi_i(\mathbf{r}) \phi_+(\mathbf{r}) d\mathbf{r} \right|^2, \quad (2)$$

where ψ_i denotes the electronic wave function, ϕ_+ the positron wavefunction, and $\mathbf{p} = \mathbf{k} + \mathbf{G}$ with \mathbf{G} a reciprocal lattice vector. $n_i(\mathbf{k})$ is the occupation function⁴³ which in the independent particle model equals 1 if the electron state i is occupied and 0 when it is empty, and the summation extends over the occupied \mathbf{k} states. In the $\rho^{2\gamma}(\mathbf{p})$ calculation, we have neglected the enhancement factor for the annihilation rate.⁴⁴ The inclusion of enhancement effects is crucial for the calculation of lifetimes but is well-known^{22,45} to be not very important for discussing questions of bonding and FS signals in momentum density. The momentum densities are calculated on a momentum mesh with step $(\delta p_x, \delta p_y, \delta p_z) = 2\pi(1/32a, 1/32a, 1/4c)$. The momentum is expressed in atomic units defined by $1/a_0$ where a_0 is the Bohr radius. The calculations include contributions from both the filled valence bands and the conduction-band which gives rise to the FS in LSCO. To study the electronic structure of the system, we consider two quantities of interest, 2D-EMD and 1D-EMD, which are the projection of EMD in 2D and 1D, respectively, given by:

$$\rho^{2d}(p_x, p_y) = \int \rho(\mathbf{p}) dp_z \quad (3)$$

and

$$\rho^{1d}(p_x) = \int \int \rho(\mathbf{p}) dp_y dp_z. \quad (4)$$

The calculated band structure of LSCO ($x = 0.3$) near the Fermi level is illustrated in Fig. 1(a). The band closest to the Fermi level is shown by the red dotted curve. This CuO_2 energy band is dominated by copper-oxygen $d_{x^2-y^2} - p_{x,y}$ orbitals. The present calculation for $x=0.3$ predicts that the vHS is above the Fermi energy, so the FS has a diamond shape closed around the Γ point. Fig. 1(b) shows the 2D momentum density contribution of the $x^2 - y^2$ band, $\rho_{x^2-y^2}^{2d}(p_x, p_y)$, together with the FS sections at $(k_z = 0)$ for the doping level $x = 0.3$ mapped periodically throughout the momentum

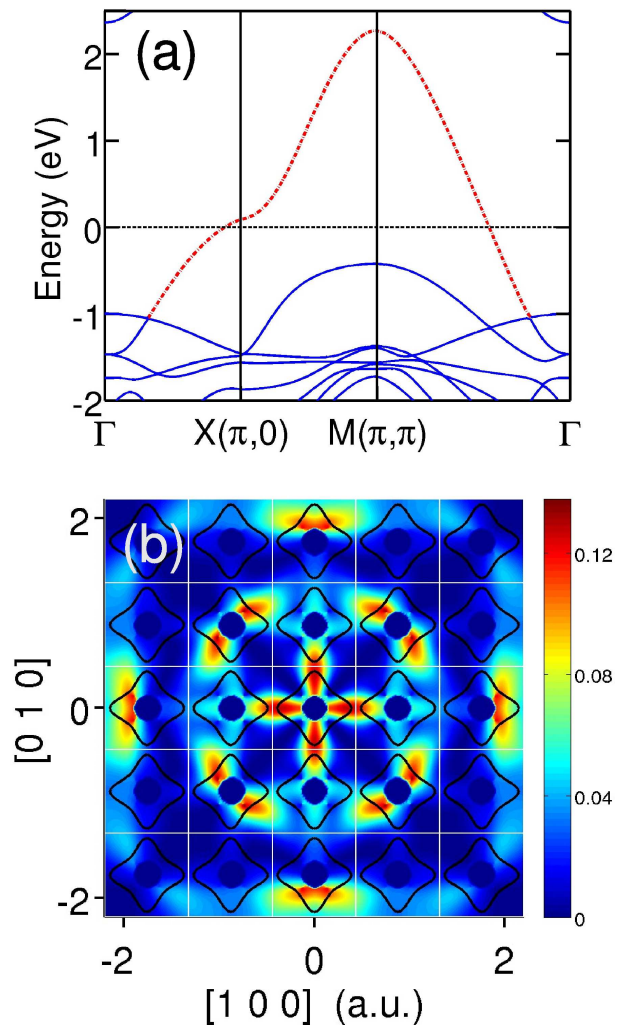


FIG. 1: (Color online) (a) Band structure of LSCO near the Fermi level. The CuO_2 band is shown as a red dotted line. (b) Calculated $\rho_{x^2-y^2}^{2d}(p_x, p_y)$ is shown together with the FS sections at $(k_z = 0)$ for the doping level $x = 0.3$. The color scale is in units of $\rho^{2d}(0,0)$. The grid represents Brillouin zones with a size of $2\pi/a$, where a is the lattice constant.

space. The Brillouin zones are visualized in the figure by a grid of $2\pi/a$, where a is the lattice constant. The momentum density acts as a matrix element on the FS map. Thus, since $\rho_{x^2-y^2}^{2d}(p_x, p_y)$ has strong amplitudes in the third Brillouin zones, the FS could be more easily detected there.

The positron annihilation and Compton scattering experiments probe all the electrons in the system. However, core and semi-core electrons give isotropic distributions while the anisotropy of the spectra is produced by electrons near the Fermi energy. Therefore, we can concentrate on analyzing the residual anisotropy after subtraction of the isotropic part. We consider an anisotropy with

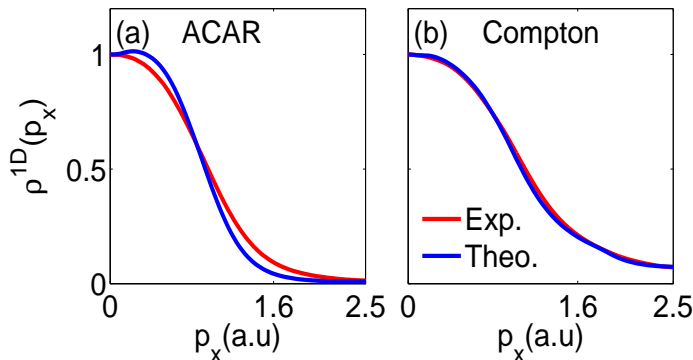


FIG. 2: (color online) Theoretical and experimental profiles $\rho^{1d}(p_x)$ for (a) ACAR and (b) Compton scattering along the [100] direction. All spectra are normalized to $\rho^{1d}(0)$.

C_{4v} symmetry, given by⁴⁶:

$$A_{C_{4v}}^{2d}(p_x, p_y) = \rho^{2d}(p_x, p_y) - \rho^{2d}\left(\frac{p_x+p_y}{\sqrt{2}}, \frac{p_x-p_y}{\sqrt{2}}\right). \quad (5)$$

In order to enhance FS signals, it is also possible to calculate another anisotropy obtained by subtraction of a smooth cylindrical average of the distribution $\rho^{2d}(p_x, p_y)$ defined by

$$A^{2d}(p_x, p_y) = \rho^{2d}(p_x, p_y) - S(\sqrt{p_x^2 + p_y^2}), \quad (6)$$

where S is a smoothed cylindrical average of ρ , in which the original spectrum is averaged over rotation angles from 0° to 45° in steps of 1° .

IV. MOMENTUM DENSITY ANISOTROPY

We start by comparing the experimental 1D profiles based on Compton scattering and ACAR measurements with the corresponding theoretical predictions. Fig. 2 shows a good level of accord between theory and experiment, especially for the Compton results. Further insight is gained by considering the 1D-projection of the anisotropy of Eq. 5 given by

$$A^{1d}(p_x) = \int_{p_a}^{p_b} A_{C_{4v}}^{2d}(p_x, p_y) dp_y, \quad (7)$$

where $\Delta p = p_b - p_a$ is the momentum range over which the projection is taken.⁴⁷ The profile $A^{1d}(p_x)$, shown in Fig. 3, is also equal to the difference of profiles²⁰ between two crystallographic directions [100] - [110] and it can be compared to a similar Compton profile anisotropy measured by Shukla *et al.* at a lower hole doping.⁴⁸ The amplitude of the theory is the same as that in the experiment, while in Ref. 48 the theoretical $A^{1d}(p_x)$ had to be scaled down by a factor of 1.4 to obtain agreement with experiment. We note that theory predicts that the

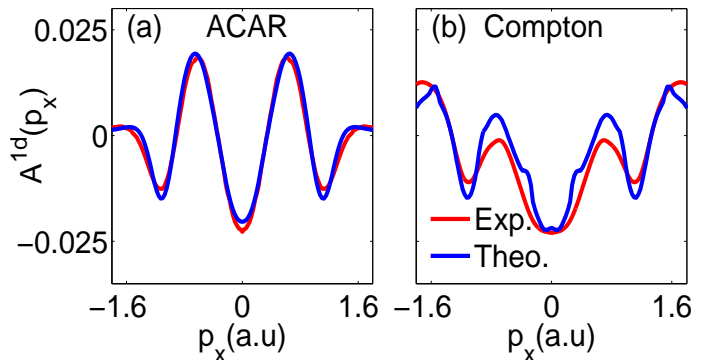


FIG. 3: (color online) Theoretical and experimental $A^{1d}(p_x)$ for (a) ACAR and (b) Compton scattering

main contribution of correlation effects is an isotropic redistribution of the momentum density,⁴⁹ so that the amplitudes of oscillation in $A^{1d}(p_x)$ become significantly reduced in the strongly correlated system. Hence our quantitative agreement between theory and experiment suggests that the $x = 0.30$ doped regime is consistent with Fermi liquid physics and that correlation effects modifying the anisotropy^{48,50} are relatively weak.

In order to focus on the Cu-O band contribution, Fig. 4 presents the 2D C_{4v} anisotropy distributions in the (p_x, p_y) plane for positron annihilation and Compton scattering spectra, respectively.⁵¹ The anisotropy of the ACAR⁵¹ in Fig. 4 can be modeled by a molecular orbital method⁵² involving the overlap of the positron wavefunction with Cu $3d$ states hybridized with O $2p$ states. For an atomic orbital, the momentum density has the same point symmetry as the corresponding charge density. This result carries over to molecular states⁵² and is equally applicable to solid-state wave functions.⁵³ The Compton scattering anisotropy maps are very similar overall to the positron-annihilation results, except that the Compton spectra extend to significantly higher momenta. This is expected since in the ACAR case the tendency of the positron to avoid positively charged ionic cores has the effect of suppressing higher momentum components of the EMD produced by the core and the localized valence electrons. Figure 4 clearly shows that the theory reproduces most of the structure observed in the measured Compton as well as positron-annihilation distributions, including the momenta at which various features are located. The fourfold symmetry of the spectra is a consequence of the symmetry of the underlying body-centered tetragonal lattice.

Therefore, an important finding of our work is that the correlations that ordinarily reduce the Compton anisotropy amplitudes are no longer effective at this doping. Similar Fermi liquid behavior has been reported in studies of overdoped Tl-cuprates.^{1,5,6} Moreover, the trend of the weakening of correlation effects with doping is also consistent with the changes observed in x-ray absorption^{54,55} and photoelectron spectroscopies.⁵⁶

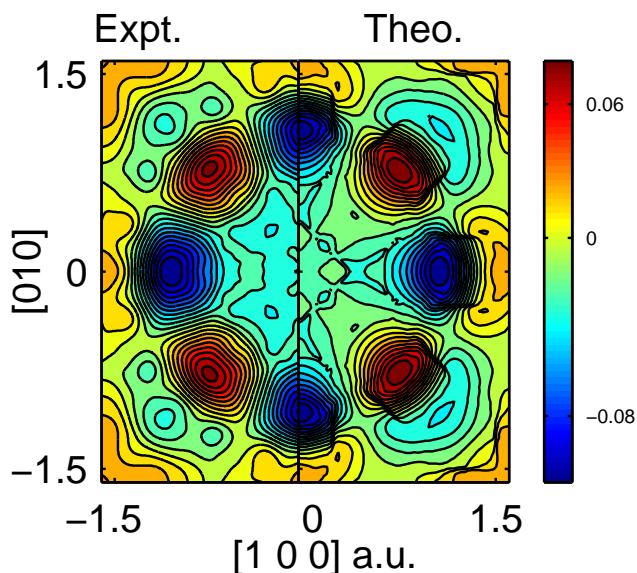
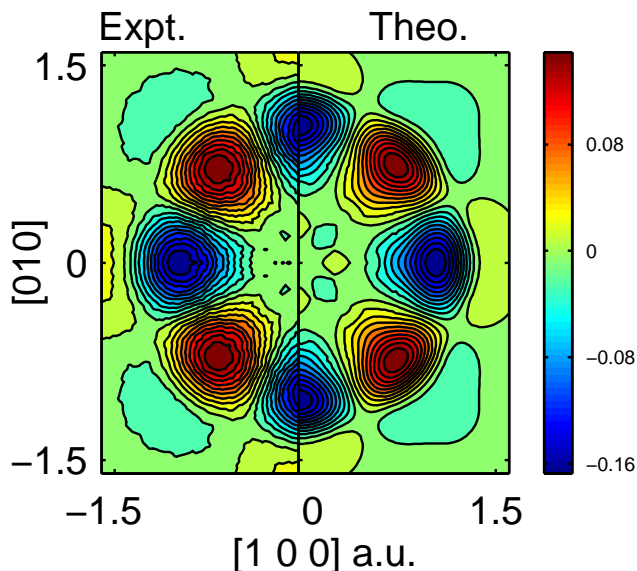


FIG. 4: (color online) Top: (left) Experimental and (right) theoretical ACAR C_{4v} anisotropy. Bottom: (left) Experimental and (right) theoretical C_{4v} anisotropy (Compton). The color scale is in units of $\rho^{2d}(0,0)$.

V. FERMI SURFACE RESULTS

We comment briefly on the positron results first. Although the electron-positron momentum density measured in a positron-annihilation experiment contains FS signatures, the amplitude of such signatures is controlled by the extent to which the positron wavefunction overlaps with the states at the Fermi energy. Fig. 5 shows the positron density distribution in a planar section of the LSCO unit cell. As in the calculation by Blandin *et al.*²², our result indicates that the positron does not probe well the FS contribution of the Cu-O planes in LSCO. Moreover, positron-annihilation favors FS contri-

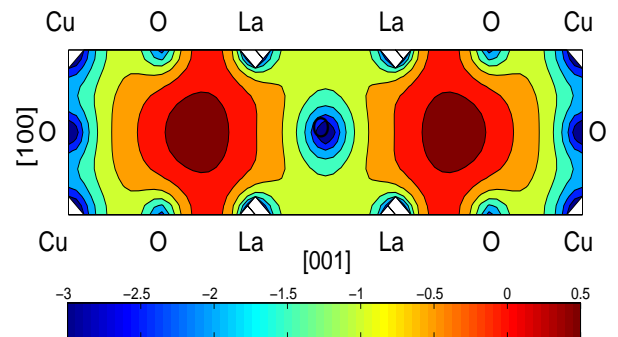


FIG. 5: (color online) Positron density for LSCO in the (010) plane. The positron wave-function is normalized in the LSCO unit cell and a logarithmic density scale (with integer numbers as units) is used in order to enhance regions with low positron density. The atomic positions (La, Cu, O) set the scale for the x and y axes.

butions involving O $2p$ rather than Cu $3d$ states because the positron wavefunction overlaps more with extended O $2p$ states compared to the more tightly bound Cu $3d$ states.

Indeed, we see little evidence of FS signatures in either the computed or the measured ACAR distributions of Fig. 3 (a). A more favorable case for the 2D-ACAR distribution is provided by the $\text{YBa}_2\text{Cu}_3\text{O}_7$ cuprate superconductor, where the 1-dimensional ridge FS has a two-fold symmetry which distinguishes it from important four-fold symmetry wave function effects.^{57,58} On the other hand, the Compton scattering calculation reveals a clear Fermi surface feature near a momentum $(1.5, 1.5)$ a.u., and equivalent positions, Fig. 4(b). Strikingly, a similar feature is seen in the experimental spectrum on the left-side of the figure. To see this more clearly, we apply a Lock-Crisp-West folding procedure, Fig. 6.

The Lock-Crisp-West (LCW) theorem⁵⁹ can be used both in Compton scattering 2D-EMD and in the case of 2D-ACAR data to study the non isotropic features of the momentum density by folding the data into a single central Brillouin zone. This technique can enhance FS discontinuities ('breaks') by coherently superposing the umklapp terms.²² However, the LCW folding can also artificially enhance errors in the experimental data.¹⁴ Thus, to more clearly expose FS features in the data, we consider the cylindrical anisotropy defined by Eq. 6. Since the subtracted function is smooth and slowly varying this procedure does not contribute to, nor create, new structures in the spectrum remaining after subtraction.

Figure 6 (a) shows the cylindrical anisotropy of the theoretical 2D-EMD spectrum. The momentum density is represented in the extended zone scheme. Because the FS is periodic, a complete FS must exist in each Brillouin zone, but with its intensity modulated by matrix element effects, as in Fig. 1(b). For a predominantly d -wave FS, the matrix elements effects will strongly suppress spectral weight near Γ , so the FS breaks are most clearly seen in higher Brillouin zones. These FS breaks

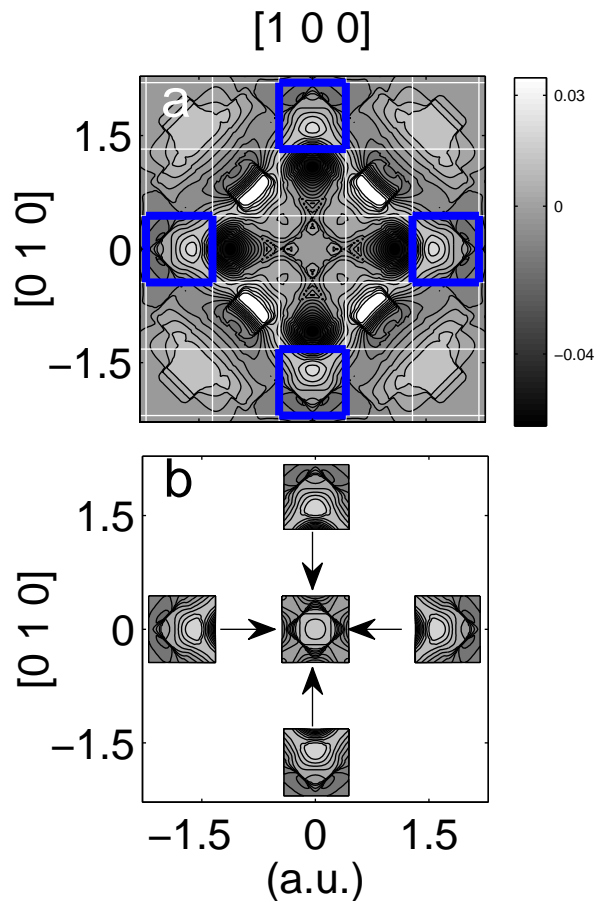


FIG. 6: (color online) (a) Cylindrical anisotropy for theoretical Compton scattering momentum density. The white lines define the Brillouin zones, while blue squares indicate a family of zones where the FS features are particularly strong. (b) The blue squared regions are isolated from the rest of the spectra and folded back to the central region. The color scale is in units of $\rho^{2d}(0,0)$.

appear superimposed on the momentum density in the form of discontinuities which can occur in any Brillouin zone. In Fig.6 (a), the Fermi surface breaks are the regions where the contours run closely together so that the electron momentum density varies rapidly at these locations. Fig.6 (a) shows the calculated Fermi breaks in several Brillouin zones. In particular, in the third zones framed with blue squares, the arc-like features are theoretically predicted FSs associated with Cu-O planes. Due to the tetragonal symmetry, a rotation of the spectrum by $\pi/2$ will generate symmetry-related regions (blue squares) with equivalent strong FS features. These regions are isolated in Fig.6 (b). By performing a ‘partial folding’, that is, folding only these regions back into the first Brillouin zone, we produce a full FS, where strong

matrix element effects are substantially circumvented. The resulting FS map is shown in the center of Fig.6 (b), and again on a larger scale in Fig.7 (a). Applying the same procedure to other Brillouin zone regions produces similar results. For instance, the four regions along the diagonal neighboring the central region can also yield full FS information, but here it is superimposed on strong momentum density features.

In Figure 7 we compare the theoretical FS obtained via the aforementioned ‘partial folding’ procedure to the corresponding experimental result. Fig.7 (a) shows that the partial backfolding technique produces the FS of correct size and topology. The same procedure when applied to the experimental spectrum yields results of Fig.7 (d). To compare with theory, we have convoluted the spectrum in Fig.7(a) with 0.07 a.u and 0.13 a.u. resolutions, leading to the distributions of Figs.7 (b) and (c) respectively. The latter is close to the actual experimental resolution used in this work.

By comparing the four frames in Fig. 7, one can see that the experimental spectrum in Fig. 7 (d) shows FS structures consistent with the LDA theory shown in Fig. 7 (a). Clearly the FS discontinuity along the nodal direction is smeared when including resolution broadening as shown in Fig.7 (b) and Fig7 (c). The best overall agreement between theory and experiment lies between Fig. 7 (b) and Fig7 (c). This is also confirmed by the cuts taken along the nodal direction plotted in Fig.8. The remaining discrepancy between experiment and theory could result from intrinsic or extrinsic inhomogeneity effects such as the appearance of local ferromagnetic clusters about concentrated regions of dopant atoms,⁸ which have been neglected in the present simulations. Our conclusion is that the closed FS for $x = 0.30$ predicted by our LDA calculation is consistent both with the present Compton scattering data and with surface-sensitive ARPES results.⁶⁰

VI. CONCLUSIONS

We have performed momentum density measurements on a high quality overdoped LSCO sample using both Compton scattering and 2D-ACAR. First principles calculations were also performed for the corresponding spectra. The quantitative agreement between the calculations and the experiment for ACAR as well as EMD anisotropies suggests that $x = 0.3$ overdoped LSCO can be explained within the conventional Fermi-liquid theory. Nevertheless, a FS signal was only clearly observed by Compton scattering in the third Brillouin zone along [100]. Our FS analysis confirms previous ARPES FS measurements⁶⁰ showing an electron-like FS in the overdoped regime. This validation is important since we provide via deep inelastic x-ray scattering experiments a truly bulk-sensitive image of momentum density maps of electrons near the Fermi level. In general, this momentum density information is difficult to extract

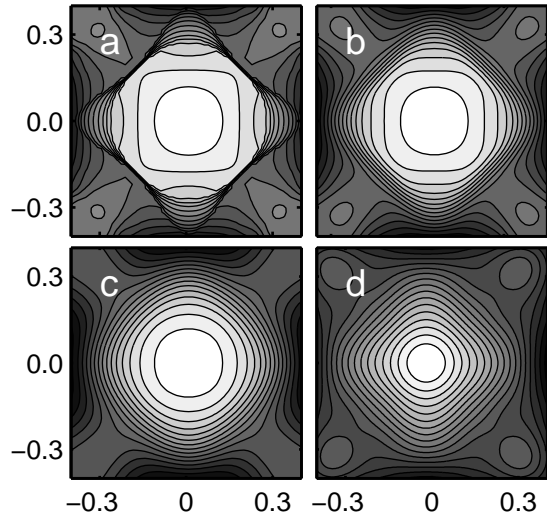


FIG. 7: Result of the 'partial folding' procedure: (a) Non convoluted Theory; (b) Theory convoluted with experimental resolution 0.07 a.u.. (c) Theory convoluted with experimental resolution 0.13 a.u.; (d) Experiment. The white color corresponds to a weight of unity (occupied) while the black color corresponds to zero (unoccupied).

from ARPES experiments due to difficulties associated with matrix element effects and the well-known surface sensitivity of ARPES.

Acknowledgements This work is supported by the USDOE grants DE-FG02-07ER46352 and DE-FG02-08ER46540 (CMSN) and benefited from the allocation of supercomputer time at NERSC and Northeastern University's Advanced Scientific Computation Center (ASCC), and the Stichting Nationale Computer faciliteiten (National Computing Facilities Foundation, NCF). The work at JASRI was supported by a Grant-in-Aid for Scientific Research (nos. 18340111 and 22540382) from the Ministry of Education, Culture, Sports, Science, and Technology (MEXT), Japan, and that at Tohoku University was supported by a Grant-in-Aid for Scientific Research (nos. 16104005, 19340090 and 22244039) from the MEXT, Japan. The Compton scattering experiments were performed with the approval of JASRI (Proposals, 2003B0762, 2004A0152, 2007B1413, 2008A1191).

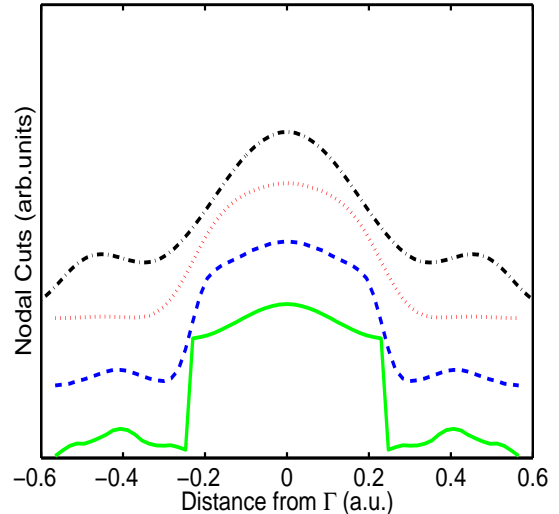


FIG. 8: (color online) Cuts of the distributions in Fig. 7 along the nodal direction. The amplitudes of theory and experiment are compared on the same scale. Curves are offset with respect to one another for clarity. From the bottom to the top, the first curve is the non-convoluted theory, the second is the convoluted theory with a resolution 0.07 a.u., the third one is the convoluted theory with a resolution 0.13 a.u. and the fourth curve is the experimental data.

- ¹ A. Damascelli, Z.-X. Shen and Z. Hussain, *Rev. Mod. Phys.* **75**, 473 (2003).
- ² K.H. Bennemann and J.B. Ketterson (Eds.), *Physics of Superconductors*, vol. 2, (Springer, Berlin, 2004).
- ³ S. Chakravarty, B.I. Halperin and D.R. Nelson, *Phys. Rev. Lett.* **60**, 1057 (1988); A. Aharony, R. J. Birgeneau, A. Coniglio, M. A. Kastner, and H. E. Stanley, *Phys. Rev. Lett.* **60**, 1330 (1988).
- ⁴ P. Fulde, *Electron Correlations in Molecules and Solids*, (Springer, Berlin, 1995).
- ⁵ C. Proust, E. Boaknin, R.W. Hill, L. Taillefer, and A.P. Mackenzie, *Phys. Rev. Lett.* **89**, 147003 (2002).
- ⁶ A. Carrington, R. A. Cooper, M. M. J. French, A. P. Mackenzie, C. Jaudet, D. Vignolles, Cyril Proust, and N. E. Hussey, *Nature* **425**, 814 (2003).
- ⁷ S.A. Kivelson, I.P. Bindloss, E. Fradkin, V. Oganessian, J.M. Tranquada, A. Kapitulnik, and C. Howald, *Rev. Mod. Phys.* **75**, 1201 (2003).
- ⁸ B. Barbiellini and T. Jarlborg, *Phys. Rev. Lett.* **101**, 157001 (2008).
- ⁹ N. Doiron-Leyraud, C. Proust, D. LeBoeuf, J. Levallois, J.B. Bonnemaïson, Ruixing Liang, D. A. Bonn, W. N. Hardy, and Louis Taillefer, *Nature (London)* **447**, 565 (2007); E.A. Yelland, J. Singleton, C. H. Mielke, N. Harrison, F. F. Balakirev, B. Dabrowski, and J. R. Cooper, *Phys. Rev. Lett.* **100**, 047003 (2008); A.F. Bangura, J. D. Fletcher, A. Carrington, J. Levallois, M. Nardone, B. Vignolle, P. J. Heard, N. Doiron-Leyraud, D. LeBoeuf, L. Taillefer, S. Adachi, C. Proust, and N. E. Hussey, *Phys. Rev. Lett.* **100**, 047004 (2008); S. C. Riggs, O. Vafek, J. B. Kemper, J. B. Betts, A. Migliori, F. F. Balakirev, W. N. Hardy, Ruixing Liang, D. A. Bonn and G. S. Boebinger *Nature Physics* **7**, 332 (2011); S.E. Sebastian, N. Harrison, P. A. Goddard, M. M. Altarawneh, C. H. Mielke, Ruixing Liang, D. A. Bonn, W. N. Hardy, O. K. Andersen, G. G. Lonzarich, arXiv:1001.5015.
- ¹⁰ T. Hanaguri, Y. Kohsaka, J.C. Davis, C. Lupien, I. Yamada, M. Azuma, M. Takano, K. Ohishi, M. Ono, and H. Takagi, *Nat. Phys.* **3**, 865 (2007).
- ¹¹ A. Bansil and M. Lindroos, *Phys. Rev. Letters* **83**, 5154(1999); A. Bansil, M. Lindroos, S. Sahrakorpi, and R. S. Markiewicz, *Physical Review B* **71**, 012503 (2005); M. Lindroos and A. Bansil, *Phys. Rev. Letters* **77**, 2985(1996).
- ¹² J. Nieminen, H. Lin, R. S. Markiewicz, and A. Bansil, *Phys. Rev. Lett.* **102**, 037001 (2009); J. Nieminen, I. Suominen, R. S. Markiewicz, H. Lin, and A. Bansil, *Phys. Rev. B* **80**, 134509 (2009).
- ¹³ D.C. Peets, J D F Mottershead, B Wu, I S Elfimov, Ruixing Liang, W N Hardy, D A Bonn, M Raudsepp, N J C Ingle and A Damascelli, *New J. Phys.* **9**, 28 (2007).
- ¹⁴ B. Barbiellini, M. Gauthier, L. Hoffmann, T. Jarlborg, A. A. Manuel, S. Massidda, M. Peter and G. Triscone, *Physica C* **229**, 113 (1994).
- ¹⁵ M. J. Cooper, P. E. Mijndarends, N. Shiotani, N. Sakai and A. Bansil in *X-Ray Compton Scattering*, Oxford University Press (2004); M. J. Cooper, *Rep. Prog. Phys.* **48**, 415 (1985).
- ¹⁶ Y. Tanaka, Y. Sakurai, A.T. Stewart, N. Shiotani, P.E. Mijndarends, S. Kaprzyk, and A. Bansil, *Phys. Rev. B* **63**, 045120 (2001); S. Huotari, K. Hamalainen, S. Manninen, S. Kaprzyk, A. Bansil, W. Caliebe, T. Buslaps, V. Honkima, and P. Suortti, *Phys. Rev. B* **62**, 7956 (2000); G. Stutz, F. Wohler, A. Kaprolat, W. Schülke, Y. Sakurai, Y. Tanaka, M. Ito, H. Kawata, N. Shiotani, S. Kaprzyk, and A. Bansil, *Phys. Rev. B* **60**, 7099 (1999).
- ¹⁷ P.E. Bisson, P. Descouts, A. Dupanloup, A.A. Manuel, E. Perreard, M. Peter and R. Sachot, *Helv. Phys. Acta* **55**, 110 (1982); J. Mader, S. Berko, H. Krakauer and A. Bansil, *Phys. Rev. Letters* **37**, 1232(1976); J. C. Campuzano, L. C. Smedskjaer, R. Benedek, G. Jennings, and A. Bansil, *Phys. Rev. B* **43**, 2788(1991).
- ¹⁸ L. P. Chan, K. G. Lynn and D. R. Harshman, *Mod. Phys. Lett. B* **6**, 617 (1992).
- ¹⁹ R.N. West, in *Positron Spectroscopy of Solids*, A. Dupasquier and A.P.Mills Jr. eds, (IOS Press, Amsterdam 1995) pp. 75-143
- ²⁰ B. Barbiellini, A. Koizumi, P. E. Mijndarends, W. Al-Sawai, Hsin Lin, T. Nagao, K. Hirota, M. Itou, Y. Sakurai and A. Bansil, *Phys.Rev. Lett.* **102**, 206402 (2009); Y. Sakurai, Y. Tanaka, A. Bansil, S. Kaprzyk, A. T. Stewart, Y. Nagashima, T. Hyodo, S. Nanao, H. Kawata, and N. Shiotani, *Phys. Rev. Letters* **74**, 2252(1995).
- ²¹ L. C. Smedskjaer, A. Bansil, U. Welp, Y. Fang and K. G. Bailey, *Physica C* **192**, 259 (1992); A.A. Manuel, A. Shukla, L. Hoffmann, T. Jarlborg, B. Barbiellini, S. Massidda, W. Sadowski, E. Walker, A. Erb and M. Peter, *J. Phys. and Chem. of Solids* **56**, 1951 (1995); A.A. Manuel, *Handbook on the Physics and Chemistry of Rare Earths Vol. 30*, edited by K.A. Gschneider, Jr., L. Eyring and M.B. Maple, (Elsevier Science B.V. 2000); P. E. Mijndarends, A. C. Kruseman, A. van Veen, H. Schut and A. Bansil, *J. Physics: Condens. Matter* **10**, 10383(1998).
- ²² P. Blandin, S. Massidda, B. Barbiellini, T. Jarlborg, P. Lerch, A. A. Manuel, L. Hoffmann, M. Gauthier, W. Sadowski, E. Walker, M. Peter, Jaejun Yu and A. J. Freeman, *Phys. Rev. B* **46**, 390 (1992).
- ²³ R. H. Howell, P. A. Sterne, M. J. Fluss, J. H. Kaiser, K. Kitazawa and H. Kojima, *Phys. Rev. B* **49**, 13127 (1994).
- ²⁴ J. Laukkanen, K. Hamalainen, S. Manninen, A. Shukla, T. Takahashi, K. Yamada, B. Barbiellini, S. Kaprzyk and A. Bansil, *J. Phys. Chem. Solids* **62**, 2249 (2001).
- ²⁵ Y. Sakurai, M. Itou, B. Barbiellini, P. E. Mijndarends, R. S. Markiewicz, S. Kaprzyk, J.-M. Gillet, S. Wakimoto, M. Fujita, S. Basak, Yung Jui Wang, W. Al-Sawai, H. Lin, A. Bansil and K. Yamada, *Science* **332**, 698 (2011).
- ²⁶ S. Wakimoto, H. Zhang, K. Yamada, I. Swainson, Hyunkyung Kim and R. J. Birgeneau, *Phys. Rev. Lett.* **92**, 217004 (2004).
- ²⁷ S. Wakimoto, Young-June Kim, Hyunkyung Kim, H. Zhang, T. Gog and R. J. Birgeneau, *Phys. Rev. B* **72**, 224508 (2005).
- ²⁸ S. Wakimoto, R. J. Birgeneau, A. Kagedan, Hyunkyung Kim, I. Swainson, K. Yamada and H. Zhang, *Phys. Rev. B* **72**, 064521 (2005).
- ²⁹ N. Hiraoka, M. Itou, T. Ohata, M. Mizumaki, Y. Sakurai and N. Sakai, *J. Synchrotron Radiat.* **8**, 26 (2001); M. Itou and Y. Sakurai, *AIP Conf. Proc.* **705**, 901 (2004); Y. Sakurai and M. Itou, *J. Phys. Chem. Solids* **65**, 2061 (2004).
- ³⁰ I. Matsumoto, J. Kwiatkowska, F. Maniawski, M. Itou, H. Kawata, N. Shiotani, S. Kaprzyk, P. E. Mijndarends, B. Barbiellini and A. Bansil, *Phys. Rev. B* **64**, 045121 (2001).

- ³¹ C. V. Falub, P. E. Mijnders, S.W.H. Eijt, M.A. van Huis, A. van Veen and H. Schut, Phys. Rev. B **66**, 075426 (2002).
- ³² S.E. Barnes and M. Peter, Phys. Rev. B **40**, 10958 (1989).
- ³³ A. Bansil, S. Kaprzyk, P. E. Mijnders and J. Toboła, Phys. Rev. B **60**, 13396 (1999).
- ³⁴ S. Sahrakorpi, M. Lindroos, R. S. Markiewicz and A. Bansil, Phys. Rev. Lett. **95**, 157601 (2005).
- ³⁵ The rigid band picture³⁶ is expected to be reasonable for doping away from the cuprate planes. It will be interesting to examine doping effects via first principles approaches³⁷.
- ³⁶ A. Bansil, Zeits. für Natur. **48** A, 165(1993); Hsin Lin, S. Sahrakorpi, R. S. Markiewicz and A. Bansil, Phys. Rev. Letters **96**, 097001 (2006); H. Asonen, M. Lindroos, M. Pessa, R. Prasad, R. S. Rao and A. Bansil, Phys. Rev. B **25**, 7075(1982).
- ³⁷ S. Kaprzyk and A. Bansil, Phys. Rev. B **42**, 7358(1990); L. Schwartz and A. Bansil, Phys. Rev. B **10**, 3261(1974); R. Prasad and A. Bansil, Phys. Rev. B **21**, 496 (1980).
- ³⁸ J. Yu, A.J. Freeman and J.-H. Xu, Phys. Rev. Lett. **58**, 1035 (2008).
- ³⁹ P. E. Mijnders and A. Bansil, Phys. Rev. B **13**, 2381 (1976); *ibid.* Phys. Rev. B **19**, 2912 (1979).
- ⁴⁰ P. E. Mijnders and A. Bansil, J.Phys.: Condens. Matter **2**, 911 (1990).
- ⁴¹ A. Bansil, R. S. Rao, P. E. Mijnders and L. Schwartz, Phys. Rev. B **23**, 3608 (1981).
- ⁴² P.E. Mijnders and A. Bansil, in *Positron Spectroscopy of Solids*, edited by A. Dupasquier and A. P. Mills (IOS Press, Amsterdam, 1995), p. 25.
- ⁴³ B. Barbiellini and A. Bansil, J. Phys. Chem. Solids **62**, 2181 (2001); B. Barbiellini, J. Phys Chem. Solids **61**, 341 (2000).
- ⁴⁴ B. Barbiellini, M. J. Puska, T. Torsti and R. M. Nieminen, Phys. Rev. B **51**, 7341 (1995); B. Barbiellini, M. J. Puska, T. Korhonen, A. Harju, T. Torsti and R. M. Nieminen, Phys. Rev. B **53**, 16201 (1996).
- ⁴⁵ B. Barbiellini, P. Genoud, P. Lerch, T. Jarlborg and M. Peter, Materials Sciences Forum **105-110**, 599 (1992).
- ⁴⁶ C_{4v} is the Schoenflies notation for a group containing a σ_v reflection in addition to C_4 , a single 4-fold axis symmetry. See e.g. M. Tinkham, *Group Theory and Quantum Mechanics*, (McGraw-Hill, 1964).
- ⁴⁷ The limits of integration are within the momentum interval [-2.5, 2.5] a.u.
- ⁴⁸ A. Shukla, B. Barbiellini, A. Erb, A.A. Manuel, T. Buslaps V. Honkimaki and P. Suortti, Phys. Rev. B **59**, 12127 (1999).
- ⁴⁹ L. Lam and P.M. Platzman, Phys. Rev. B **9**, 5122 (1974).
- ⁵⁰ B. Barbiellini and P.M. Platzman, Mat. Sci. Forum **255-257**, 189 (1997).
- ⁵¹ Our experimental ACAR spectra are in reasonable accord with earlier studies Refs. 22,23.
- ⁵² P.E.A. Turchi, A.L. Wachs, K.L. Wetzler, J.H. Kaiser, R.N. West, Y.C. Jean, R.H. Howell and M.J. Fluss, J. Phys. Condens. Matter **2**, 1635 (1990).
- ⁵³ R. Harthoorn and P.E. Mijnders, J. Phys. F **8**, 1147 (1978).
- ⁵⁴ T. Ahmed, T. Das, J.J. Kas, Hsin Lin, B. Barbiellini, Fernando D. Vila, R.S. Markiewicz, A. Bansil and J. J. Rehr, Phys. Rev. B **83** 115117 (2011).
- ⁵⁵ D. C. Peets, D. G. Hawthorn, K. M. Shen, Y.-J. Kim, D. S. Ellis, H. Zhang, S. Komiya, Y. Ando, G. A. Sawatzky, R. Liang, D. A. Bonn and W. N. Hardy, Phys. Rev. Lett. **103**, 087402 (2009).
- ⁵⁶ M. Schneider, R.-S. Unger, R. Mitdank, R. Müller, A. Krapf, S. Rogaschewski, H. Dwelk, C. Janowitz and R. Manzke, Phys. Rev. B **72**, 014504 (2005).
- ⁵⁷ H. Haghghi, J. H. Kaiser, S. Rayner, R. N. West, J. Z. Liu, R. Shelton, R. H. Howell, F. Solal, P. A. Sterne and M. J. Fluss, Phys. Rev. Lett. **67**, 382 (1991).
- ⁵⁸ L. Hoffmann, A.A. Manuel, M. Peter, E. Walker, M. Gauthier, A. Shukla, B. Barbiellini, S. Massidda, Gh. Adam, S. Adam, W. N. Hardy and Ruixing Liang, Phys. Rev. Lett. **71**, 4047 (1993).
- ⁵⁹ D.G. Lock, V.H.C. Crisp and R.N. West, J. Phys. F **3**, 561 (1973).
- ⁶⁰ T. Yoshida, X.J. Zhou, M. Nakamura, S.A. Kellar, P.V. Bogdanov, E.D. Lu, A. Lanzara, Z. Hussain, A. Ino, T. Mizokawa, A. Fujimori, H. Eisaki, C. Kim, Z.X. Shen, T. Kakeshita and S. Uchida, Phys. Rev. B **63**, 220501 (2001); T. Yoshida, X. J. Zhou, K. Tanaka, W. L. Yang, Z. Hussain, Z. X. Shen, A. Fujimori, S. Sahrakorpi, M. Lindroos, R. S. Markiewicz, A. Bansil, Seiki Komiya, Yoichi Ando, H. Eisaki, T. Kakeshita and S. Uchida, Phys. Rev. B **74**, 224510 (2006).